International Journal of Pharmaceutics 570 (2019) 118631

Contents lists available at ScienceDirect

International Journal of Pharmaceutics

journal homepage: www.elsevier.com/locate/ijpharm

Dual chamber cartridges in a continuous pharmaceutical freeze-drying concept: Determination of the optimal dynamic infrared heater temperature during primary drying

Laurens De Meyer[a], Joris Lammens[b], Brecht Vanbillemont[a], Pieter Jan Van Bockstal[a], Jos Corver[a], Chris Vervaet[b], Wolfgang Friess[c], Thomas De Beer[a,*]

[a] Laboratory of Pharmaceutical Process Analytical Technology, Department of Pharmaceutical Analysis, Faculty of Pharmaceutical Sciences, Ghent University, Ottergemsesteenweg 460, 9000 Ghent, Belgium
[b] Laboratory of Pharmaceutical Technology, Department of Pharmaceutics, Faculty of Pharmaceutical Sciences, Ghent University, Ottergemsesteenweg 460, 9000 Ghent, Belgium
[c] Department of Pharmacy, Pharmaceutical Technology and Biopharmaceutics, Ludwig-Maximilians-Universitaet, Munich, Germany

ARTICLE INFO

Keywords:
Continuous freeze-drying
Dual chamber cartridge
Infrared radiation
Choked flow
Spin freezing

ABSTRACT

The applicability of DCCs in a continuous freeze-drying concept based on spin freezing and infrared heating was evaluated. Maximum applicable filling volume was evaluated. Secondly the mechanistic model for the determination of the optimal dynamic infrared heater temperature during primary drying of regular vials during continuous freeze-drying was adapted and validated for DCCs. Finally, since spin frozen DCCs may be more prone to choked flow due to the small neck opening and the large product surface area, it was evaluated if the choked flow constraints in the model could be increased to improve the efficiency of the drying process. The experiments revealed that the maximum allowable filling volume for spin freezing at the current experimental setup was 0.8 ml which is 80% of the maximum filling volume. Applying the mechanistic model for the determination of the optimal dynamic infrared heater temperature during primary drying of the studied DCCs and experimentally verifying this determined infrared heater temperature trajectory resulted in an elegant freeze-dried product without visual signs of collapse. The experimentally determined primary drying time agreed with the one calculated based on the mechanistic model. Choked flow did not occur during the continuous freeze-drying of DCCs containing 3% sucrose or 3% mannitol.

1. Introduction

The importance of biopharmaceuticals for the pharmaceutical industry is rising together with a trend to move from large volume drug product manufacturing towards the production of low volume/high value drug products. Approximately 50% of these biopharmaceutical drug products are stabilized by freeze-drying (Costantino and Pikal, 2004; Rey and May, 2010).

Freeze-drying is a low temperature drying process, based on the principles of mass and heat transfer, employed to convert solutions of (heat) labile materials into solids having sufficient stability for distribution and storage (De Meyer et al., 2015).

Freeze-drying is a batch process and consists of three consecutive steps: freezing, primary drying and secondary drying (Wang, 2000; Rey and May, 2010; Jennings, 1999). The aseptically filled containers are loaded on the shelves of the freeze-dryer. The freezing step is initiated by decreasing the shelf temperature to approximately −40 °C or lower. Most of the water in the formulation crystallizes into ice hereby concentrating the solutes (freeze-concentration). These solutes can either crystallize at the eutectic temperature (T_{eu}) or concentrate further until a glass is formed at the glass transition temperature of the maximally freeze-concentrated amorphous matrix (T_g') (Kasper and Friess, 2011). When the liquid formulation is completely solidified (eventually after an included annealing step), a vacuum, in general between 10 and 30 Pa, is introduced. During primary drying, sublimation starts once the chamber pressure is below the triple point of water. The temperature of

* Corresponding author.
E-mail addresses: Laurens.DeMeyer@UGent.be (L. De Meyer), Joris.Lammens@UGent.be (J. Lammens), Brecht.Vanbillemont@UGent.be (B. Vanbillemont), pieterjan.vanbockstal@ugent.be (P.J. Van Bockstal), Jos.Corver@RheaVita.nl (J. Corver), Chris.Vervaet@UGent.be (C. Vervaet), wolfang.friess@lrz.uni-muenchen.de (W. Friess), Thomas.DeBeer@UGent.be (T. De Beer).
URL: http://www.ugent.be/fw/pharmaceutical-analysis/en/research/pat (L. De Meyer).

https://doi.org/10.1016/j.ijpharm.2019.118631
Received 2 April 2019; Received in revised form 12 August 2019; Accepted 17 August 2019
Available online 20 August 2019
0378-5173/

Nomenclature

γ	adiabatic constant for triatomic gas (–)
ΔH_s	latent heat of ice sublimation (51139 J/mol)
ρ_{wv}	density of the water vapour (kg/m^3)
ϕ	volume fraction of ice (–)
ϵ	emission coefficient of the emitting surface (–)
α	absorptivity of the target surface (–)
A_p	surface area of spin frozen product (m^2)
c	speed of sound for an ideal gas (m/s)
$d_{d,o}$	diameter of the DCC neck opening (m)
h_f	height of the spin frozen product (m)
M	molar mass of water (kg/mol)
$\dot{m}_{max}$	maximum sublimation rate (kg/s)
$\dot{m}_{sub}$	sublimation rate (kg/h)
P_{rad}	power provided by IR heater to spin frozen DCC (W)
P_{sub}	power required for sublimation (W)
P_{sur}	power provided by surroundings to spin frozen DCC (Pa)
$P_{w,c}$	partial vapour pressure in the freeze-drying chamber (Pa)
$P_{w,i}$	partial vapour pressure at the sublimation front (Pa)
R	gas constant (8.3144621 J/(mol K))
R_p	dry product mass transfer resistance (m/s)
$r_{d,i}$	inner radius of the DCC (m)
$r_{d,o}$	outer radius of the DCC (m)
$r_{p,i}$	radius from the DCC center to the border of the spin frozen layer (m)
s	distance radiator to center DCC (m)
T_c	collapse temperature (K)
T_{eu}	eutectic temperature (K)
T_i	product temperature at the sublimation front (K)
T_g'	glass transition temperature of the maximum freeze-concentrated formulation (K)
T_{rad}	infrared heater temperature (K)
T_{wv}	temperature of the water vapour (K)
V	filling volume (m^3)
V_{max}	maximum volume flow of sublimed gas (m^3/s)
$v_{sound,safe}$	safe velocity of sound (m/s)

the shelves is increased to supply the energy for sublimation. The product temperature at the sublimation front (T_i) has to be kept below the collapse temperature (T_c) for an amorphous product or the T_{eu} in case of a crystalline product during the entire primary drying process to avoid cake collapse. Secondary drying is the final step of the freeze-drying process. Therewith, the vacuum is remained and the shelf temperature is increased to remove the remaining unfrozen water by desorption (Pikal, 2002).

Traditional freeze-drying, as performed till now in the pharmaceutical industry, has always been a batch process and little to no significant technology innovations were made (Ganguly et al., 2013). The batch process is characterized by several disadvantages like the uncontrolled ice nucleation during the freezing step or the uneven heat transfer in the drying chamber leading to vial-to-vial and batch-to-batch variability. It is also not possible to monitor and control the process at vial level due to the close packing of the vials on the freeze-dryer shelves making it impossible to implement probes to monitor every single vial. The relatively thick layer thickness and small product surface area together with the non dynamic freeze-drying conditions create an inefficient process. Furthermore loading and unloading the freeze-dryer makes a large and expensive clean room space necessary. This inefficiency of the batch freeze-drying process makes it a time consuming and expensive process. The disadvantages and shortcomings of batch-wise freeze-drying have been described in more detail in De Meyer et al. (2015), De Meyer et al. (2017), Van Bockstal et al. (2016) and Van Bockstal (2016).

To overcome these disadvantages and to meet the most recent regulatory guidelines like the Quality-by-Design (QbD) and Process Analytical Technology (PAT) framework of the United States Food and Drug Administration (FDA), a continuous freeze-drying process has been developed (United States Food and Drug Administration, 2004). This continuous freeze-drying process guarantees a shorter and more efficient freeze-drying process, a lower ecological footprint due to a much smaller sterile and particle controlled environment and a uniform product quality where every single container is monitored and controlled through the entire process (Corver, 2013).

The developed continuous freeze-drying concept introduces three major differences compared to conventional batch freeze-drying (Fig. 1). Firstly the freezing step, during which the vials are spun around their longitudinal axis, creating a uniform, thin frozen product layer at the vial wall (i.e. spin freezing). Herewith, the solution is solidified by a flow of temperature controlled, sterile gas. The resulting thinner product layer and the larger surface area of the spin frozen product significantly contribute to improving the efficiency of the drying process. The second major difference is the drying step where energy is homogeneously and in a controlled way supplied, either by conduction (e.g. electric heating pad) or radiation (e.g. infra-red heater), towards the vial wall where the product layer is located (De Meyer et al., 2015; De Meyer et al., 2017; Van Bockstal et al., 2016; Van Bockstal, 2016).

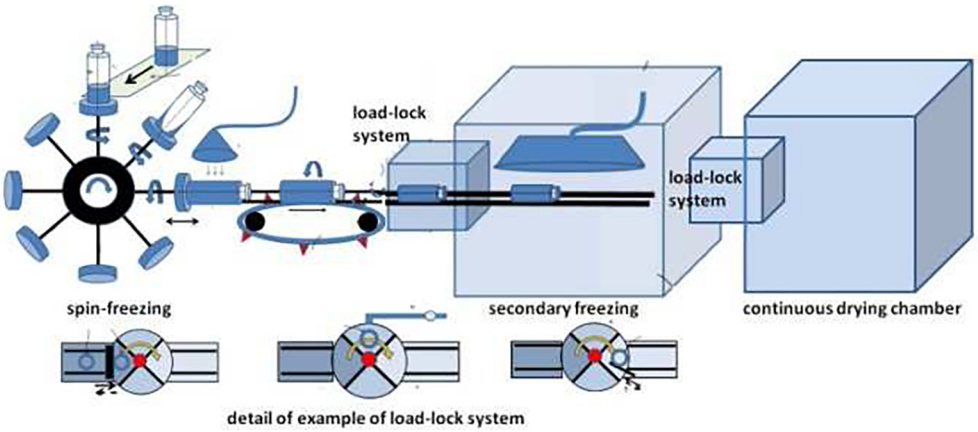

Fig. 1. Schematic illustration of a continuous freeze-dryer. The process starts with a spin freezing step after which the vial is transported through a load-lock system to a continuous drying chamber. A secondary freezing chamber can be implemented for an annealing step.

The third difference is the continuous flow of vials between the different modules (i.e., spin freezing, annealing and drying) of the continuous freeze-dryer separated by load-locks. Each vial is processed as an individual batch where the status of each vial is monitored and controlled (Corver, 2013).

The continuous freeze-drying process is extensively described in previous work from the authors De Meyer et al. (2015), De Meyer et al. (2017), Van Bockstal (2016).

For traditional pharmaceutical batch freeze-drying, the most used container type is a single dose glass vial (Rey and May, 2010). Before the lyophilised product can be administered (e.g. injected) to the patient, it has to be reconstituted with water for injection by the health care practitioner. This reconstitution procedure bears the risks of dosing errors, needle stick injuries and microbial contamination.

The pharmaceutical industry has the intention to reduce the number of handling steps required for reconstitution by using prefilled syringes and auto injectors (Werk et al., 2016). It is not only a life cycle management strategy to differentiate new and established products but self-administration also has lower costs for health care payers and the dosing compliance is improved. Genotropin (recombinant human growth hormone manufactured by Pfizer) was one of the first lyophilised protein formulations that transitioned from standard vials to dual chamber cartridges (DCCs) as primary packaging container (Rey and May, 2010). DCCs are an alternative type of container system for freeze-dried products. DCCs consist of a hollow glass cylinder which consists of two chambers separated by a rubber plunger and a rear plunger to close the liquid compartment. One chamber contains the freeze-dried formulation whilst the other chamber contains the reconstitution liquid (Fig. 2).

When an external force is applied to the rear plunger, it moves together with the middle plunger allowing the liquid to flow from the reconstitution liquid chamber via the bypass to the freeze-dried product chamber to reconstitute the product. The DCC container system has many advantages compared to a traditional glass vial: it is easier to reconstitute, has a better dose accuracy and a lower risk of microbial contamination (Werk et al., 2016; Werk et al., 2016; Korpus et al., 2015). Despite the advantages of DCCs, the application of traditional batch lyophilisation is challenging since the small contact area between the DCC and the freeze-dryer shelves and the longer distance between the shelf and the liquid formulation in the DCC, results in a poor conductive heat transfer and thus increased freeze-drying time. Besides this, all other disadvantages of traditional batch freeze-drying, as described above, are also applicable on the batch freeze-drying process of DCCs.

Several efforts were done by creating customized holder systems to protect the DCC against tipping over and to improve the heat transfer during the freeze-drying process (Korpus et al., 2016; Korpus and Friess, 2017). Four categories of holder systems are commonly used in the DCC freeze-drying industry. Block systems, where holes are drilled in an aluminum block to contain a DCC are the first category. When an individual holder is used for each DCC, it is called a “shell system”. A third type is the “flexible holder” where the DCCs are hanging in a plate above the shelf. The guardrail holder is the final category and is a bulk system in which the DCCs are tightly packed next to each other (Korpus and Friess, 2017). These efforts improved the heat transfer during the freeze-drying process but the disadvantages of batch freeze-drying still remain present.

The continuous pharmaceutical freeze-drying process already proved to reduce the duration of freeze-drying at a vial level with a factor 10–40 and even more depending on the vial dimensions and formulation characteristics (De Meyer et al., 2015; Van Bockstal et al., 2016; Van Bockstal, 2016). This process could eliminate the challenges inherently coupled to batch freeze-drying of DCCs. The DCC-to-DCC and batch-to-batch variability is eliminated and it is possible to monitor and control the process at the DCC level. The process efficiency is increased by spin freezing the DCC resulting in a thin layer thickness and a large surface area.The use of infrared heating as energy transfer mechanism circumvents the poor conductive heat transfer as observed during batch freeze-drying.

The continuous freeze-drying topic is trending and other research groups try to catch the wave. Hosokawa Micron BV developed the “Active Freeze-drying Technology” for bulk freeze-drying. Active freeze-dryers have an improved heat transfer rate since the product is moving during the process hence resulting in a shorter drying step because dried product is removed and does not hinder sublimation. All process steps are done in a single processing unit (Van Der Wel Peter, xxxx). Efforts are done to convert this technique in a continuous process where dried power is continuously removed from the processing unit. Nevertheless, this process is only applicable for bulk powder production. This is a major drawback since dosing accuracy is very important and liquid dosing has a higher accuracy compared to powder filling. The research group of Roberto Pisano recently started doing research about continuous freeze-drying based on suspended vials (Pisano and Capozzi, 2017). Not much information is publicly available at this time of writing but the concept depends on the movement of suspended vials in a nucleation module and a drying module. The product is located as a plug at the bottom of the vial. Controlled nucleation helps to reduce the dry product resistance and shorten the drying process. Another promising concept for continuous pharmaceutical freeze-drying in the future is microwave-assisted freeze-drying. The process is already well-known in the food industry thanks to its rapid drying characteristics. The technique is based on the capability of a material to absorb microwaves and convert them into thermal energy by molecular interactions with the electromagnetic field (Gitter et al., 2018). An international patent is pending claiming the formulation and production of thermostable dried vaccine formulations using microwave vacuum drying (Bhanbhani et al., 2015). Gitter et al. freeze-dried a monoclonal antibody by using microwave-assisted freeze-drying and were able to obtain a 77% percent overall drying time reduction making it applicable in a continuous concept (Gitter et al., 2018).

2. Objectives

The aim of this study was to find out whether it is possible to continuously freeze-dry DCCs via the recently presented continuous freeze-drying process based on spin freezing and infrared heating, herewith overcoming the disadvantages inherently coupled to batch freeze-drying of DCCs.

The maximum applicable DCC filling volume, resulting in a homogeneous uniform layer thickness without liquid spill during spinning, was evaluated in a first step. Second, the mechanistic model for the determination of the optimal dynamic IR heater temperature during primary drying of regular vials described by Van Bockstal (2016) was adapted and validated for the DCCs. Finally, since DCCs may be more prone to choked flow due to the small neck opening and the large product surface area, it was evaluated if the choked flow safety factor, implemented in the mechanistic model, could be increased for DCCs to improve the efficiency of the drying process.

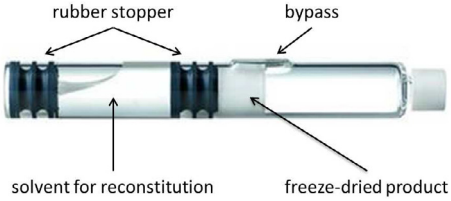

Fig. 2. Schematic illustration of a dual chamber cartridge containing the freeze-dried product and the solvent for reconstitution (Skinsorb, 2018).

3. Materials and methods

Two different model formulations were used. Formulation 1 consisted of mannitol 30 mg/ml, sucrose 3.42 mg/ml, glycine 3.75 mg/ml and sodium chloride 0.58 mg/ml. Formulation 2 only consisted of 30 mg/ml sucrose. Mannitol, sucrose and glycine were purchased from Sigma–Aldrich (Saint Louis, MO, USA). Sodium chloride was purchased from Fagron (Waregem, Belgium).

The DCC (Nipro Glass Germany AG, Munnerstadt, Germany) used in this study has an inner diameter of 8.60 mm, an outer diameter of 10.81 mm, a total DCC height of 79.4 mm and an inner neck diameter of 2.30 mm. The height of the upper compartment containing the freeze-dried product is 32 mm. The plungers were made of bromobutyl rubber (FM457-0, Helvoet Pharma, Lommel, Belgium). In traditional batch freeze-drying of DCCs, a maximum filling volume of 1.0 ml was used for this type of DCC.

3.1. Experimental setup

Spin freezing DCCs was done by installing a DCC in a drill whereafter the DCC was rotated around its longitudinal axis at approximately 2900 rotations per minute (rpm) creating an equally spread product layer on the inner DCC wall. Whilst spinning, the rotating DCC was immersed in liquid nitrogen for 30 ± 5 s to completely solidify the product.

After spin freezing, the DCC was transferred to the rotation stage (see Fig. 3) located in the drying chamber of an AMSCO Finn-Aqua GT4 freeze-dryer (GEA, Köln, Germany). The rotating DCC is located in front of an IR heater (Weiss Technik, Zellik, Belgium) at a distance of 4.0 cm measured between the center of the DCC and the center of the IR heater.

3.2. Spin freezing dual chamber cartridges

Based on the inner DCC radius ($r_{d,i}$) and the radius of the DCC neck opening ($r_{d,n}$) the theoretical maximum product layer thickness (l_{max}) during spinning can be determined by:

$$l_{max} = r_{d,i} - r_{d,n} \quad (1)$$

The volume corresponding to this layer thickness can be calculated by:

$$V_f = \pi h_f (r_{d,i}^2 - r_{d,n}^2) \quad (2)$$

with h_f the height of the spin frozen product (m), $r_{d,i}$ the inner DCC radius (m) and $r_{d,n}$ the radius of the DCC neck opening (m).

To determine the maximum possible filling volume in the DCC without spilling during spinning, the DCC, filled with the volume of demineralised water as calculated by Eq. (2), was installed in the drill applied for spin freezing whereafter the DCC was horizontally rotated around its longitudinal axis at approximately 2900 rotations per minute (rpm) creating an equally spread product layer on the inner DCC wall. The DCC was in a horizontal position during spinning to minimize the difference in layer thickness between the top and bottom of the DCC due to gravitation. The DCC neck was surrounded by a paper cylinder to allow the detection of any liquid spill.

To evaluate whether it was possible to spin freeze a DCC resulting in a homogeneous product layer thickness, the DCC filled with the experimentally determined maximum filling volume was spun and subsequently, whilst spinning, immersed in liquid nitrogen for 30 ± 5 s to completely solidify the product. After spin freezing the product, the plunger was removed and the homogeneity of the frozen layer thickness was visually evaluated.

3.3. Determination of the optimal dynamic IR heater temperature during primary drying of DCCs

The mechanistic model described in Van Bockstal et al. allowing as fast as possible drying of regular vials without the product temperature exceeding the collapse temperature (Van Bockstal, 2016) was adapted for DCCs.

Primary drying consists of two phases. During the first part of the primary drying process, the pressure in the drying chamber was decreased until the desired chamber pressure (in this study) of 13.3 Pa was reached. Chamber pressure was fixed during the optimization process since it has no influence on radiative heat transfer (Ganguly et al., 2010). The fastest sublimation rates can be obtained by decreasing the chamber pressure as much as possible. The value of 13.3 Pa was chosen since this chamber pressure could easily be obtained and maintained during the freeze-drying process. Until the desired chamber pressure was reached, the IR heaters were turned off. The mass of ice which sublimed during the initial pressure decrease, due to energy from the surroundings, was experimentally determined (see Section 3.4).

The second part of the primary drying process starts once the desired chamber pressure was reached and the IR heaters were activated. During sublimation, the sublimation front moves towards the DCC wall and the dried product layer increases in thickness. In traditional freeze-drying, a two-dimensional approach is necessary to model the primary drying step since the sublimation front is not planar. In the case of continuous freeze-drying, a one-dimensional approach can be used as the product forms a thin layer at the cylindrical DCC wall. The end-effects, being the energy transfer from the vial to the product at the bottom and top of the DCC, were excluded in the mechanistic model since the effect was small due to the small layer thickness and the large surface area available for sublimation.

When determining the maximum possible sublimation rate during primary drying, several limitations have to be taken into account.

The first limitation of the sublimation rate is the dry product resistance (R_p) of the formulation. Sublimation of the ice crystals creates a network of pores in the dried product. These pores create a resistance towards the water vapour generated at the sublimation front. When more water vapour is generated than the amount that can be transferred through the dried layer, the water vapour pressure at the sublimation front will increase. As the water vapour pressure is related to T_i

Fig. 3. Experimental set up for freeze-drying a DCC positioned on a rotary stage and in front of the infrared heater.

(Eq. (7)), an uncontrolled increase of T_i is inevitable which can result in undesired cake collapse.

The sublimation rate $\dot{m}_{sub}$ (kg/s) is given by:

$$\dot{m}_{sub} = \frac{A_p}{R_p}(P_{w,i} - P_{w,c}) \tag{3}$$

with Ap the surface area of the spin frozen product (m^2), R_p the dry product resistance (m/s), $P_{w,i}$ the water vapour pressure above the sublimation front (Pa) and $P_{w,c}$ the partial water vapour pressure in the drying chamber (Pa). During primary drying, the composition of the gas in the drying chamber consists almost entirely of water vapour (Fissore et al., 2011). Therefore it is assumed that $P_{w,c}$ is equal to the overall pressure in the drying chamber.

The surface area of the product during primary drying A_p is given by:

$$A_p = 2\pi h_f (r_{p,i} + l) \tag{4}$$

with h_f the height of the spin frozen product layer in the DCC (m), l the dried layer thickness (m) and $r_{p,i}$ the radius from the center of the DCC to the border of the spin frozen layer (m), which is given by:

$$r_{p,i} = \sqrt{r_{d,i}^2 - \frac{V}{\pi h_f}} \tag{5}$$

with $r_{d,i}$ the inner DCC radius (m), V the filling volume (m^3) and h_f the height of the spin frozen product layer (m).

R_p, another parameter in Eq. (3), depends on the thickness of the dried product layer l (m).

The following equation describes the link between R_p (m/s) and the dried layer thickness l (Fissore et al., 2009):

$$R_p = R_{p,0} + \frac{A_{Rp} l}{1 + B_{Rp} l} \tag{6}$$

with $R_{p,0}$ (m/s), A_{Rp} (1/s) and B_{Rp} (1/m) parameters, which are dependent on the composition of the freeze-dried product, its concentration and the freezing step (Kochs et al., 1993; Searles et al., 2001; Hottot et al., 2007). These parameters are determined experimentally by fitting to experimental data.

R_p increases when l increases during the primary drying step (Eq. (8)). In order to keep T_i below the collapse temperature of the product, in most cases the energy input needs to decrease during primary drying.

The driving force for ice sublimation is the pressure difference between the water vapour pressure at the sublimation front $P_{w,i}$ and the water vapour pressure in the freeze-dryer chamber $P_{w,c}$ which can be adjusted.

$P_{w,i}$ is calculated by the Clausius-Clapeyron equation (Overcashier et al., 1999):

$$P_{w,i} = 3.6\ 10^{12} e^{\frac{-6145}{T_i}} \tag{7}$$

with T_i the product temperature at the sublimation front (K).

To optimize the drying efficiency without losing an elegant cake structure, T_i is targeted to be equal to – but not exceeding – the glass transition temperature T_g' during the entire sublimation step.

In most cases, T_c is several degrees higher than T_g' as the high viscosity of the sample close to T_g' prevents viscous flow (Kasper and Friess, 2011).

Finally, the increase in the dried layer thickness (Δl) for a specified time interval Δt (s) is given by:

$$\frac{\Delta l}{\Delta t} = \frac{\dot{m}_{sub}}{A_p \rho_{ice} \phi} \tag{8}$$

with $\dot{m}_{sub}$ the sublimation rate (kg/s), A_p the surface area of the product (m^2), ρ_{ice} the density of ice (kg/m^3) and ϕ the volume fraction of ice (–).

The second limitation of the sublimation rate next to R_p is the choked flow limit. Choked flow is described as a loss of pressure control at the level of the DCC neck or at the level of the duct connecting the chamber with the condenser (Patel et al., 2010). Choked flow is discussed in detail in Section 3.5.

Choked flow occurs once the speed of the vapour flow through the container opening or chamber duct approaches the speed of sound (Mach 1). A further increase in mass flow would result in an elevated water vapour density and thus local pressure increase inside the container or drying chamber with a subsequent increase of product temperature. The maximum allowable $\dot{m}_{sub}$ is thus limited by the speed of sound. A gas however should be considered as being compressible at gas speeds higher than 0.3 Mach (Anderson, 2007). Therefore, a safety factor (Eq. (10)) of 0.3 is introduced to calculate the maximal speed of the gas flow ($v_{sound,safe}$) to avoid compression effects.

The choked flow condition is calculated with the following equations:

$$c = \sqrt{\frac{\gamma R T_{wv}}{M}} \tag{9}$$

$$v_{sound,safe} = 0.3c \tag{10}$$

$$V_{max} = v_{sound,safe} \pi (d_{d,n}/2)^2 \tag{11}$$

$$\dot{m}_{max} = V_{max} \rho_{wv} \tag{12}$$

with c the velocity of sound (m/s), γ the adiabatic constant for a triatomic gas (–), R the molar gas constant (J/mol K), T_{wv} the temperature of the water vapour, M the molar mass of water (kg/mol), $v_{sound,safe}$ the safe velocity of sound (m/s), V_{max} the maximum volume of sublimed gas (m^3/s), $d_{d,n}$ the diameter of the DCC neck opening (m), $\dot{m}_{max}$ the maximum mass of sublimed gas (kg/s) and ρ_{wv} the density of the water vapour (kg/m^3).

The density of the water vapour ρ_{wv} (kg/m^3) is given by:

$$\rho_{wv} = \frac{P_{w,i} M}{R T_{wv}} \tag{13}$$

with $P_{w,i}$ the water vapour pressure above the sublimation front (Pa), M the molar mass of water (kg/mol), R the molar gas constant (J/mol K) and T_{wv} the temperature of the water vapour (K).

$\dot{m}_{sub}$ (calculated by Eq. (3)) has to be compared with $\dot{m}_{max}$ to ensure the choked flow criterium is not violated. If $\dot{m}_{sub}$ would be higher than $\dot{m}_{max}$, $\dot{m}_{sub}$ is to be fixed at $\dot{m}_{max}$ in Eq. (3). To allow determination of the number of times this choked flow limit was reached and thus $\dot{m}_{sub}$ was limited, a choked flow counter was implemented in the model. Every time the choked flow limit was reached, the choked flow counter was increased with one unit.

Based on $\dot{m}_{sub}$, the power (P_{tot}, W) that should be provided to the vial to sublime the ice can be calculated:

$$P_{tot} = \frac{\dot{m}_{sub} \Delta H_s}{M} \tag{14}$$

with $\dot{m}_{sub}$ the sublimation rate (kg/s) and ΔH_s the latent heat of ice (J/mol).

It should also be taken into account that part of the power comes from the surroundings, as the walls and door of the freeze-dryer chamber have a higher temperature than the frozen DCC. Therefore, P_{tot} is compensated for the radiation energy from the surroundings:

$$P_{rad} = P_{tot} - P_{sur} \tag{15}$$

with P_{rad} the power that should be supplied by the IR heater to the DCC (W) and P_{sur} the power originating from the surroundings and supplied to the DCC (W). The temperature of the IR heater T_{rad} necessary to provide sufficient energy to achieve the optimal sublimation rate is calculated by the Stefan-Boltzmann law:

$$P_{rad} = A_{rad} F \sigma (\epsilon T_{rad}^4 - \alpha T_{DCC}^4) \tag{16}$$

with A_{rad} the area of the emitting surface (m^2), F the view factor (–) (the fraction of radiation emitted by the IR heater hitting the glass vial (Nellis and Klein, 2009)), σ the Stefan-Boltzmann constant

(5.67×10^{-8} W/(m^2 K^4)), ϵ the emission coefficient of the emitting surface (0.93, −), T_{rad} the temperature of the emitting surface (K), α the absorptivity of the target surface (0.93, −) and T_{DCC} the temperature of the spin frozen DCC (K). In general, α is estimated as the value of ϵ for the target surface (see Table 1) (Bird et al., 2006).

The view factor F was calculated based on the Monte Carlo methodology described by Brenner (Brenner, 2010). The walls and door of the freeze-drying chamber are together with the IR heater considered as diffuse emitters. This means their surfaces emit radiation uniformly in all directions. The view factor only depends on the relative geometric orientation of the emitting surface (i.e. IR heater or chamber wall/door) to the spin frozen container which are represented by a flat plate and a cylinder respectively (Van Bockstal, 2016). The view factor is determined by simulating a defined amount of rays (N) generated from random positions on the emitting surface at randomly chosen angles (Nellis and Klein, 2009). For each generated ray, the evaluation was made whether it will hit the target surface (i.e. the container wall) directly or not. F is then estimated by taking the ratio between the number of target hits to the total amount of emitted rays, N.

The mechanistic model is described in detail by Van Bockstal (2016). The input parameters which are used in the mechanistic model, are listed in Table 1.

The mechanistic model allows calculating the optimal dynamic IR heater temperature as function of primary drying time to obtain the most efficient primary drying process without exceeding the choked flow limit and the T_g' of the formulation. The optimal dynamic IR heater temperature trajectory was calculated and applied to the drying process of the two model formulations. Experimental verification of the calculated primary drying trajectory was done by visual inspection of the cake structure (e.g. meltback and collapse) and determination of the residual moisture after freeze-drying DCCs after 90, 100 and 110% of the calculated drying time.

3.4. Determination of the radiation energy contributed by the surroundings

A DCC, filled with 0.8 ml of demineralized water; was spin frozen as described in Section 3.1 and transferred to the drying chamber in front of the inactivated IR heater. The amount of ice which sublimed during the initial pressure decrease from atmospheric pressure to 13.3 Pa was determined gravimetrically. The average time to reach the desired vacuum was 7 min.The power corresponding with the amount of ice sublimed was calculated via Eq. (14). The experiment was conducted in triplicate.

In a next experiment, the vacuum was maintained for an extra 10 min after reaching 13.3 Pa without activation of the IR heater. After this time period, the mass of sublimed ice was determined gravimetrically. The experiment was conducted in triplicate. Based on Eq. (14), the power which corresponds to this mass of sublimed ice was calculated.

The difference in power between both experiments reflects the energy provided through radiation from the surroundings to the spin frozen DCC (Van Bockstal, 2016).

3.5. Influence of choked flow during primary drying of DCCs

Choked flow is described as a loss of pressure control due to a container or equipment limitation, more specific at the level of the DCC neck or at the level of the duct connecting the chamber of the freeze-dryer with the condenser (Patel et al., 2010). Choked flow occurs once the speed of the vapour flow through the container opening or chamber duct approaches the speed of sound, where a further increase in mass flow would result in an elevated vapour density in the container or drying chamber, leading to a local pressure increase inside the container or drying chamber and subsequent product temperature increase. The water vapour flow has to go through the neck of the container and subsequently through the duct between the drying chamber and the condenser. The container neck or the duct can limit the vapour flow (e.g. choked flow) when the diameter is insufficient to allow vapour flow without pressure increase. It is important to notice that choked flow is a restriction of the speed of the gas but not the flow rate of the gas. A higher flow rate at the choked flow gas speed can be obtained by compression of the gas.

For batch freeze-drying, the duct connecting the freeze-drying chamber with the condenser is the most critical point where choked flow can occur; more precisely at the narrowest point of the duct, being the valve separating the drying chamber from the condenser.

During sublimation, the water vapour flow through the container (vials, DCCs, etc) neck opening is rather low due to the low sublimation rate during batch freeze-drying but the freeze-dryer itself contains a lot of containers creating a high gas flow at the condenser duct. When the diameter of the duct is too small to allow a vapour flow without compression of the gas, choked flow occurs.

During continuous freeze-drying, the amount of containers being processed at the same time in the continuous freeze-drying equipment is much smaller compared to batch freeze-drying, but the gas flow through the container neck is much higher compared to batch freeze-drying due to the larger product surface area where sublimation takes place. The risk of choked flow is higher for DCCs than for vials due to the smaller DCC neck opening.

3.6. Thermal imaging

The temperature of the rotating spin frozen DCC was monitored continuously during the primary drying step using a FLIR A655sc IR thermal camera (FLIR Systems Inc, Wilsonville, United States) to detect the temperature increase at the sublimation front due to choked flow. The glass DCC wall temperature is measured by the thermal camera. Based on this measurement and taking into account the temperature gradient over the glass wall and the ice layer, the temperature at the sublimation front can be determined (Van Bockstal et al., 2018). A choked flow induced temperature increase at the sublimation front will result in a temperature increase of the outer glass DCC wall which will be detected by the thermal camera.

The thermal camera is equipped with an uncooled micro-bolometer as detector. The camera was placed outside the freeze-drying chamber in front of an IR transparent germanium window (3 mm thickness with anti-reflectance coating) in the chamber door (Fig. 4). The IR heater was located in the freeze-dryer at an angle of 90° to the thermal camera. The focal length of the camera was 13.1 mm. The thermal resolution was 30 mK Noise Equivalent Temperature Difference (NEDT). A

Table 1
Nominal values of the DCC specific input parameters to calculate the dynamic temperature profile of the infrared heater during primary drying.

Parameter	Numerical value
Input parameters view factor computation	
Length radiator	0.045 m
Width radiator	0.045 m
DCC outer diameter $r_{d,o}$	0.0108 m
Height of DCC	0.079 mm
Distance between DCC center and IR heater	0.040 m
Number of simulated rays (Monte Carlo simulation)	10^6
Temperature walls	288.95 K
Input parameters for calculating the dynamic temperature profile	
Temperature shelves	263.15 K
Emissivity quartz glass (IR heater) ϵ	0.93
DCC inner diameter $r_{d,i}$	0.0086 m
DCC neck diameter $d_{d,n}$	0.0023 m
Height of the spin frozen product layer h_f	0.0310 m
Filling volume V	0.8 mL
Volume fraction ice ϕ	1
View factor F	0.0501

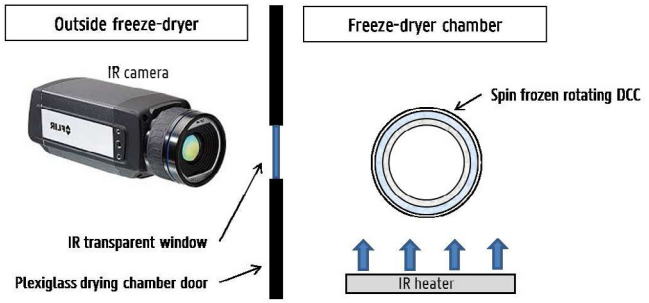

Fig. 4. Schematic illustration of the thermal imaging setup (top view) during primary drying. The spin frozen DCC is rotating in front of the IR heater located inside the freeze-dryer chamber. The thermal camera is located outside measuring through an IR transparent window (FLIR A655sc, 2018).

thermal image was captured every 30 s via the FLIR ResearchIR MAX Software (FLIR Systems Inc, Wilsonville, United States). Data processing was conducted by using the same software package. The emissivity of the glass vial was 0.93 (Bird et al., 2006).

4. Results and discussion

4.1. Spin freezing of dual chamber cartridges

Based on Eq. (1), the maximum theoretical product layer thickness for the tested DCC type was 3.14 mm (distance between inner glass DCC wall and DCC neck opening) which was equivalent to a filling volume of 1.68 ml (Eq. (2)). When rotating a DCC containing this volume, a liquid spill was detected on the paper cylinder. In the current experimental spinning setup it was not possible to perfectly align the DCC and hereby eliminating the precession and vibration which caused the liquid spill. The slow rotation speed combined with the small radius of the DCC may result in a centrifugal force which is not sufficient to create a uniform thin product layer at the vial wall. Together with the vibration and precession this could result in the liquid spill. In a well built spin freezer, the DCC is perfectly aligned and the theoretically calculated maximum filling volume of 1.68 ml should be possible. In the current spinning device, the maximum filling volume for this type of DCC was found to be 0.8 ml. This volume was therefore used for all other experiments described in this paper. Based on visual inspection, a homogeneous layer thickness was obtained after spin freezing 5. Since the DCC was in a horizontal position during spinning and freezing, no deviation in layer thickness between the bottom and top of the DCC occurred.

4.2. Determination of the radiation energy contributed by the surroundings

The amount of ice which sublimed during the initial pressure decrease from atmospheric pressure to 13.3 Pa was 0.00478 g ± 0.00072 g. The power contributed by the surroundings was calculated after compensation for the initial ice sublimation during the initial pressure decrease. The net mass of sublimed ice of a DCC containing 0.8 ml of demineralised water with inactivated IR heater after 10 min under vacuum (13.3 Pa) was 0.0820 g ± 0.0014 g which corresponds, based on Eq. (14), to an experimental P_{sur} of 0.3898 W.

4.3. Determination of the optimal dynamic IR heater temperature during primary drying of DCCs

The model developed by Van Bockstal (2016) to determine the optimal dynamic IR heater temperature during primary drying of spin frozen regular vials allowing as efficient as possible drying without exceeding T_g' was re-calibrated for the DCC specific parameters (see Table 1). For both model formulations, the dynamic IR heater temperature for the optimal primary drying trajectory of the studied DCCs was calculated herewith assuring that T_g' was not exceeded and that choked flow was avoided.

The optimal dynamic temperature of the IR radiator (T_{rad}) is plotted in function of the primary drying time (Fig. 6) for both model formulations.

The predicted primary drying time for Formulation 1 was 1 h 41 min and 1 h 36 min for Formulation 2. The calculated optimal dynamic IR heater temperature profiles were apparently constant for both formulations. The choked flow counter, which was implemented in the model and counts how many times the choked flow limit was reached during the determination of the optimal drying trajectory, reached a value of 606 for Formulation 1 and 576 for Formulation 2. The specified time interval Δt (Eq. (8)) for the determination of the optimal dynamic temperature profile was 10 s. The value of 606 and 576 indicated that every time interval Δt of the primary drying step, the choked flow limit was reached and the maximal sublimation rate was limited (606 x 10s = 6060 s = 1 h 41 min; 576 × 10 s = 5760 s = 1 h 36 min) (Eq. (12)). To limit the sublimation rate and hereby avoiding choked flow, the energy input was decreased during the entire primary drying process hence resulting in a constant IR heater temperature profile.

Different drying times and IR heater temperatures can be noticed in Fig. 6 for both model formulations (1 h 41 min and 1 h 36 min for Formulation 1 and Formulation 2 respectively) due to the difference in R_p. The R_p of Formulation 2 is higher compared to Formulation 1 (Kuu et al., 2006) and therefore it was expected that the IR heater temperature was higher during primary drying of Formulation 1. The IR heater temperature trajectory in Fig. 6 on the contrary showed a higher IR heater temperature for Formulation 2. The explanation can be found in the energy input limitation to prevent choked flow. When applying a safety factor of 0.3, the sublimation rate was limited during the whole primary drying step for both formulations. $\dot{m}_{sub}$ was therefore equal for both formulations. Based on Eq. (3), this means $P_{w,i}$ should differ for both formulations and thus also T_i (Eq. (7)). Therefore the calculated energy input for Formulation 1 was lower than the energy input for Formulation 2.

When this IR heater temperature profile was applied during primary drying of a spin frozen DCC containing 0.8 ml for both formulations, the drying process resulted in an elegant cake without visual signs of collapse. Formulation 1 was used for the experimental verification. Karl Fischer analysis revealed a residual moisture content of 2.39 ± 0.12 % (n = 3). The visual cake aspect and residual moisture was also determined at 90% and 110% of the calculated primary drying time (91 min and 111 min respectively). For the 90% drying time, during aeration, parts of the freeze-dried cake melted indicating that primary drying was not completely finished. This was also confirmed by the Karl Fischer data which revealed a higher residual moisture content of 6.30 ± 0.80% (n = 3).

Extending the drying time to 110% (111 min) did not significantly reduce the residual moisture level compared to the 100% set point of 101 min, also resulting in elegant cakes. This confirms the completion of primary drying at the calculated time.

4.4. Influence of choked flow during primary drying of DCCs

Application of the mechanistic model to determine the optimal

Fig. 5. Visual aspect of the DCC after spin freezing (right) and cross sectional view after removal of the middle plunger (left).

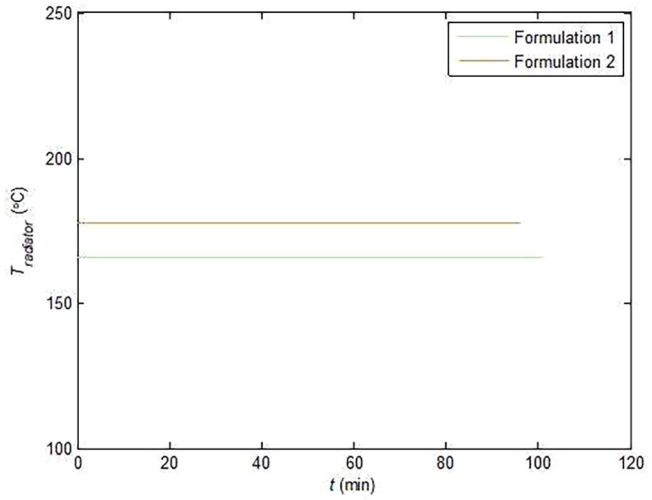

Fig. 6. Dynamic infrared heater temperature as function of primary drying time calculated for a choked flow safety factor of 0.3. The end of the line is the calculated end of primary drying.

dynamic IR heater temperature during primary drying of DCCs resulted in a constant optimal IR heater temperature for both model formulations at the safety factor of 0.3. The safety factor which was used in the mechanistic model (as used in Eq. (10)), was increased to 1.0 in order to evaluate if compression effects occurred at gas speeds higher than 0.3 Mach but lower than Mach 1 as described by Anderson (2007). By increasing the safety factor, it could also be evaluated if it was possible to dry the spin frozen DCC more efficiently. By changing the safety factor (from 0.3 to 1.0) for the applied DCC re-calibrated mechanistic model, the optimal IR heater temperature in function of primary drying time was calculated for both model formulations (Fig. 7). At a safety factor of 1.0, the maximum allowable water vapour flow was set just below the speed of sound. When compression of the gas occurred in the DCC, it was hypothesized that melt-back or collapse of the product would be present due to a product temperature increase hereby exceeding T_g' or T_c.

When implementing the 1.0 safety factor, the choked flow limit was reached for the mannitol containing Formulation 1 during the first 500 s of primary drying resulting in a stationary optimal IR heater temperature during this period to avoid choked flow and hence collapse. For Formulation 2, when applying a safety factor of 1.0, it was impossible to reach a sublimation rate resulting in a gas vapour flow through the DCC neck which equals the speed of sound. When performing the freeze-drying cycle for both formulations with their calculated optimal IR heater temperature trajectory as visualised in Fig. 8, no signs of melt-back or collapse were visible. This indicates that for Formulation 2, the product temperature did not exceed the T_g' due to compression effects in the DCC. As Anderson et al. described that a gas should be considered as compressible at gas speeds higher than 0.3 Mach, it was expected that a local pressure increase inside the DCC could occur resulting in a temperature increase at the sublimation front. Since the effects of gas compressibility above 0.3 M were not visualized as collapse or melt-back, it could be concluded that compression of the gas was absent or that the degree of gas compression was small hereby not resulting in a temperature increase at the sublimation front with cake collapse or melt-back as a result. This can not be concluded for Formulation 1 due to the mannitol in the formulation. When the product temperature exceeds T_g', the crystalline mannitol hinders visual detection of cake collapse.

Experimental verification of the calculated primary drying time for Formulation 1 at a 1.0 safety factor revealed a residual moisture level of 1.45 ± 0.29% after 100% (n = 3) of the calculated primary drying time (33 min). A drastic reduction in primary drying time is obtained by increasing the choked flow safety factor from 0.3 to 1.0. No visual signs of melt back or collapse were visually observed (Fig. 8).

The visual cake aspect and residual moisture was also determined at 90 and 110% of the calculated primary drying time (30 min and 36 min respectively). For the 90% drying time, during aeration, parts of the freeze-dried cake melted indicating that primary drying was not completely finished (Fig. 8). This was also confirmed by the Karl Fischer data which revealed a residual moisture content of 6.65 ± 1.34% (n = 3). The 110% drying time resulted in an elegant cake aspect without visual signs of collapse. The residual moisture content was 1.67 ± 0.24% (n = 3). This result confirmed that primary drying was finished at 100% of the calculated primary drying time.

Applying a higher safety factor, allowed the determination of a sublimation rate without taking into account the choked flow constraint. It was expected that the by choked flow induced temperature increase would result in cake collapse or melt-back when sublimation rates were created which resulted in a water vapour flow higher than the speed of sound. Increasing the choked flow safety factor to 1.5 allowed calculating the optimal dynamic IR heater temperatures during primary drying without respecting the choked flow limit and more specific to reach a water vapour flow higher than the speed of sound (Eq. (10)).

The results of the determination of the optimal dynamic IR heater temperature trajectory when applying a safety factor of 1.5 are shown in Fig. 9. For Formulation 1, the constant IR heater temperature during the first 500 s of primary drying when applying a safety factor of 1.0 was deleted and becomes dynamic (Fig. 9).

Since a choked flow safety factor of 1.0 already resulted in a dynamic infrared heater temperature without reaching the choked flow limit, the increase in choked flow safety factor from 1.0 to 1.5 had no influence on the heater temperature during primary drying of Formulation 2.

Applying the calculated infrared heater settings as visualized in Fig. 9 for Formulation 1 should induce choked flow during primary drying and thus an increase in product temperature with a possibility of exceeding the T_g'. However, it was not possible to visually detect collapse due to the crystalline mannitol cake. Therefore the product temperature was monitored continuously during primary drying of Formulation 1 under these conditions with a thermal camera. Taking a closer look at the thermogram (Fig. 10), during the first 10 min, the product temperature increased due to the temperature ramp up of the IR heater, the increase of R_p and the increase of T_i towards T_g' (Van Bockstal et al., 2018). After this timespan, the IR heater reached its steady state temperature. No temperature increase above the T_g'

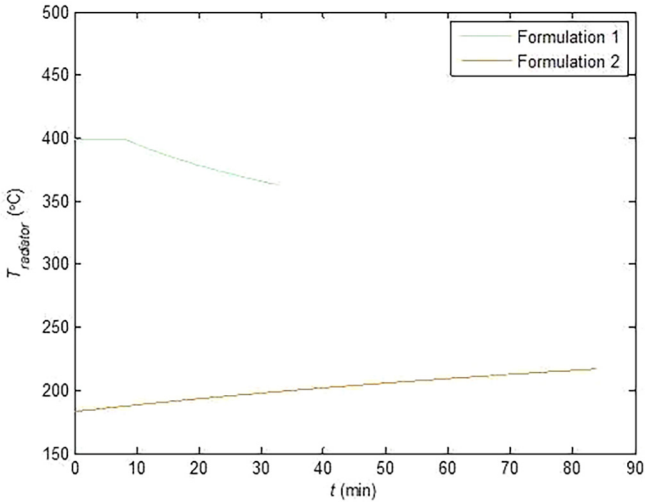

Fig. 7. Dynamic infrared heater temperature as function of primary drying time calculated for a choked flow safety factor of 1.0.

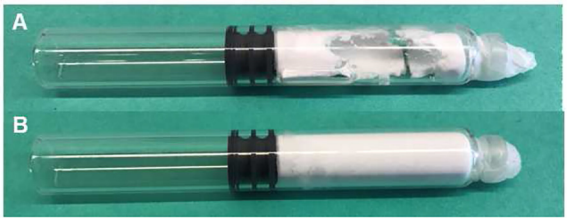

Fig. 8. A: visual cake aspect of Formulation 1 after 90% of primary drying time. Remaining ice melted during aeration. B: visual cake aspect of Formulation 1 after 100% of primary drying time. No visual signs of collapse were present.

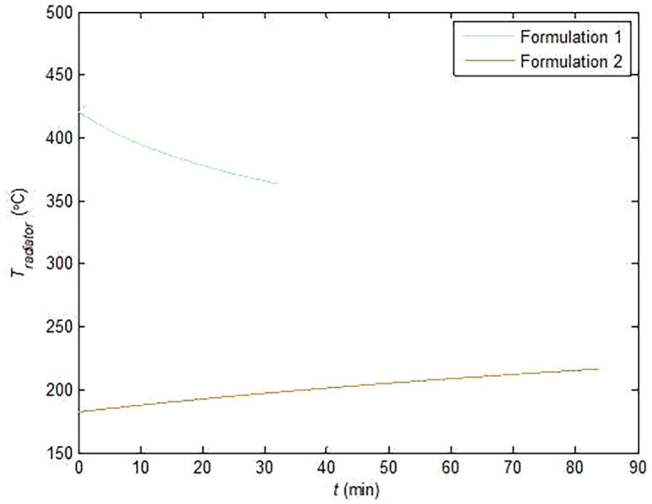

Fig. 9. Dynamic infrared heater temperature as function of primary drying time calculated for a choked flow safety factor of 1.5.

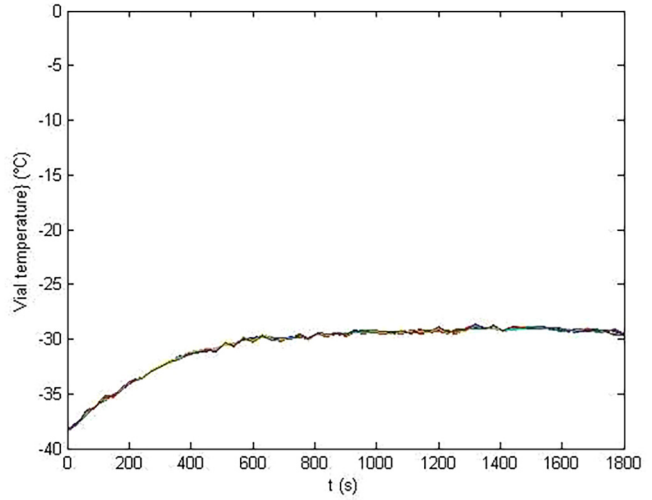

Fig. 10. Temperature of the outer vial wall during the primary drying step of a spin frozen DCC in function of the primary drying time.

followed by a temperature decrease was observed. It was expected that when choked flow occurs (i.e. during the first 500 s of primary drying), the pressure would increase in the DCC leading to a decrease in the driving force of sublimation ($P_{w,i}$-$P_{w,c}$) (Eq. (3)). As a result, the sublimation rate would decrease but the energy input from the IR heater was calculated for the higher sublimation rate resulting in an increase of T_i since not all energy input could be used for sublimation and would thus heat up the product. After the first 500 s the lower energy input from the IR heater resulted in a sublimation rate and water vapour flow below the speed of sound. T_i will decrease since the optimal dynamic IR temperature was determined to obtain a T_i just below T_g'.

These data imply the absence of choked flow in the DCC. The temperature profile in Fig. 10 is the normal trajectory during primary drying without choked flow. The absence of choked flow when applying the optimal dynamic IR heater temperature trajectory allowing choked flow can be explained by the IR heater characteristics. It was assumed in the mechanistic model that the IR heater is able to reach its set temperature immediately at the start of the primary drying process. Experiments however revealed that the IR heater was characterized by a temperature ramp up when activated. Thus the actual temperature of the IR heater at the start of primary drying was lower than calculated by the model. It takes five to eight minutes for the IR heater to reach its initial temperature of 420 °C and this time frame corresponds to the first 500 s of the primary drying step where choked flow occurs.

The only case where choked flow could occur was when the spin frozen DCC was placed in front of an activated IR heater at steady state temperature at the start of primary drying. Due to practical limitations, it was not possible to simulate this situation in the batch freeze-dryer. However, in the continuous freeze-drying prototype, a frozen vial will be placed in front of an already activated IR heater. In this case, choked flow could occur during the first 500 s of primary drying.

Another possible explanation for the absence of melt-back or collapse could be found in the different importances of the pressure between traditional batch freeze-drying and continuous freeze-drying based on spin freezing. When taking a closer look at choked flow during traditional batch freeze-drying, choked flow occurs at the level of the duct connecting the freeze-dryer chamber and the condenser. As a consequence, the pressure inside the freeze-dryer chamber will increase. This pressure increase results in a higher energy transfer from the shelves towards the container since the energy transfer via convection will become more important. On the other hand, the driving force for sublimation, being the difference in partial vapour pressure between the sublimation front ($P_{w,i}$) and the freeze-dryer chamber ($P_{w,c}$), will decrease due to the higher chamber pressure. These two factors will result in an increasing product temperature leading to collapse and melt-back of the product.

When choked flow occurs during continuous freeze-drying, it will take place at the level of the container neck opening. The high sublimation rate and large surface area of the frozen product will result in a high mass flow of water vapour through the DCC neck opening possibly resulting in choked flow. Since the choked flow occurs at the container neck opening, the subsequent pressure increase takes place inside the container. This implies there is no increase in energy transfer towards the DCC. As long as the driving force for sublimation ($P_{w,i}$–$P_{w,c}$) remains positive, sublimation will take place. A slight product temperature increase could be noticed as the driving force becomes smaller due to pressure increase in the container but as long as the product temperature does not exceed the T_c, no melt-back or collapse is noticed. Since the continuous freeze-drying process is a fast process with primary drying times of one or two hours, the increase in product temperature is not fast enough to violate the T_c.

A further increase in choked flow safety level (> 1.5) was not applicable due to R_p and T_g' limitations. The higher IR heater temperatures coupled to this increased choked flow safety factor would induce collapse due to exceeding of T_g' by the high energy input rather than a temperature increase resulting from choked flow.

Based on these results it could be concluded that it was not possible to induce the detrimental effects of choked flow in a DCC containing 0.8 ml of the mannitol containing formulation. The pressure rise in the DCC due to choked flow, did not cause the temperature at the sublimation front to rise beyond the limits of T_g'.

Applying the continuous freeze-drying process on DCCs significantly reduces the primary drying time. Literature reports primary drying times of 10 h (75 mg/ml Bovine Serum Albumin, V = 0.8 ml) (Werk et al., 2016), 34.6 h (2 mg/ml mAb, V = 0.5 ml) and 56 h (100 mg/ml

mAb, V = 0.5 ml) during batch freeze-drying of DCCs (Korpus and Friess, 2017). These primary drying times are in sharp contrast with the primary drying times obtained by the continuous process (i.e. 32 min (30 mg/ml mannitol, V = 0.8 ml) and 84 min (30 mg/ml sucrose)).

It can be concluded that a choked flow safety factor of 1.0 is safe to implement in the mechanistic model without risking a collapsed product. Even higher safety factors are possible but the product temperature has to be monitored during the freeze-drying process to prevent an increase of the product temperature with the risk of product collapse or melt-back when exceeding the T_c.

5. General conclusion

It was possible to spin freeze a DCC containing 0.8 ml obtaining a homogeneous frozen thin product layer covering the entire DCC wall. The applicable filling volume is dependent of the type of DCC used and the alignment of the spin freezer. The mechanistic model to calculate the optimal dynamic IR heater temperature during primary drying as described by Van Bockstal et al. is adapted to the dimensions of the DCC and the position of the DCC in front of the infrared heater and in the freeze-dryer chamber. In a first setting, a limitation to the maximum sublimation rate taking potential choked flow at the DCC opening was taken into account. Verification of this calculated optimal IR heater trajectory revealed a good visual cake aspect without any visual signs of macroscopic cake collapse and with an acceptable residual moisture content. In a second setting the choked flow limitation was changed to improve the primary drying efficiency and shorten the primary drying time. A drastic reduction in primary drying time was obtained for the formulation with the crystalline bulking agent (33 min instead of 101 min) and no effects of choked flow could be substantiated. Monitoring the product temperature during primary drying to detect the presence of choked flow did not reveal a choked flow induced temperature increase at the time frame where choked flow was predicted by the mechanistic model. This was explained by the temperature ramp up of the infrared heater at the start of primary drying whereas the model assumes a direct steady state temperature. It was not possible to induce choked flow in the current experimental continuous freeze-drying setup. Therefore, for this setup, a safety factor of 1.0 can be used to calculate the choked flow limit without any risk of cake collapse or melt-back.

Declaration of Competing Interest

The authors declare that they have no known competing financial interests or personal relationships that could have appeared to influence the work reported in this paper.

Acknowledgements

Research funded by a PhD fellowship SB (1S23417N: Brecht Vanbillemont) of the Research Foundation Flanders (FWO).

References

Anderson, J.D., 2007. Fundamentals of Aerodynamics, fourth ed. McGraw - Hill, New York.
Bhanbhani, A., Evans, R., Sinacola, J., Jones, M., 2015. Method of obtaining thermostable dried vaccine formulations (WO 2015/057541 A1).
Bird, R.B., Stewart, W.E., Lightfoot, E.N., 2006. Transport Phenomena. John Wiley & Sons Inc, New York.
Brenner, J., 2010. Design Specifications for Wet-bulb Aspirator Apparatus. University of Wisconsin - Madison (Ph.D. thesis).
Corver, J., 2013. Method and system for freeze-drying injectable compositions, in particular pharmaceutical compositions WO2013036107.
Costantino, H., Pikal, M., 2004. Lyophilization of biopharmaceuticals.
De Meyer, L., Van Bockstal, P.J., Corver, J., Vervaet, C., Remon, J.P., De Beer, T., 2015. Evaluation of spin freezing versus conventional freezing as part of a continuous pharmaceutical freeze-drying concept for unit doses. Int. J. Pharm. 496.
De Meyer, L., Lammens, J., Mortier, S.T.F., Vanbillemont, B., Van Bockstal, P.J., Corver, J., Nopens, I., Vervaet, C., De Beer, T., 2017. Modelling the primary drying step for the determination of the optimal dynamic heating pad temperature in a continuous pharmaceutical freeze-drying process for unit doses. Int. J. Pharmaceutics.
Fissore, D., Pisano, R., Velardi, S., Barresi, A., Galan, M., 2009. PAT tools for the optimization of the freeze-drying process. Pharmaceutical Eng. 29.
Fissore, D., Pisano, R., Barresi, A.A., 2011. Advanced approach to build a design space for the primary drying of a pharmaceutical freeze-drying process. Int. J. Drug Develop. Res. 100 (11), 4922–4933.
FLIR A655sc. 2018. URLhttps://www.flir.com/products/a655sc/.
Ganguly, A., Nail, S.L., Alexeenko, A.A., 2010. Experimental determination of the key heat transfer mechanisms in pharmaceutical freeze drying. School of Aeronautics and Astronautics Faculty Publications 27.
Ganguly, A., Alexeenko, A.A., Schultz, S.G., Kim, S.G., 2013. Freeze-drying simulation framework coupling product attributes and equipment capability: toward accelerating process by equipment modifications. Eur. J. Pharm. Biopharm. 85.
Gitter, J., Geidobler, R., Presser, I., Winter, G., 2018. Significant drying time reduction using microwave-assisted freeze-drying for a monoclonal antibody. J. Pharm. Sci.
Hottot, A., Vessot, S., Andrieu, J., 2007. Freeze drying of pharmaceuticals in vials: Influence of freezing protocol and sample configuration on ice morphology and freeze-dried cake texture. Chem. Eng. Process. 46.
Jennings, T., 1999. Lyophilization: introduction and basic principles, vol. 25.
Kasper, J.K., Friess, W., 2011. The freezing step in lyophilization: Physico-chemical fundamentals, freezing methods and consequences on process performance and quality attributes of biopharmaceuticals. Eur. J. Pharm. Biopharm. 78.
Kochs, M., Körber, C., Heschel, I., Nunner, B., 1993. The influence of the freezing process on vapour transport during sublimation in vacuum-freeze-drying of macroscopic samples. Int. J. Heat Mass Transf. 36.
Korpus, C., Friess, W., 2017. Evaluation of different holder devices for freeze-drying in dual-chamber cartridges with a focus on energy transfer. J. Pharm. Sci. 106 (4), 1092–1101.
Korpus, C., Friess, W., 2017. Lyophilization cycle design for dual chamber cartridges and a method for online process control: the ”DCC LyoMate” procedure. J. Pharm. Sci. 106 (8), 2077–2087.
Korpus, C., Haase, T., Sönnichsen, C., Friess, W., 2015. Energy transfer during freeze-drying in dual-chamber cartridges. J. Pharm. Sci. 104 (5), 1750–1758.
Korpus, C., Pikal, M., Friess, W., 2016. Heat transfer analysis of an optimized, flexible holder system for freeze-drying in dual chamber cartridges using different state-of-the-art PAT tools. J. Pharm. Sci. 105 (11), 3304–3313.
Kuu, W.Y., Hardwick, L.M., Akers, M.J., 2006. Rapid determination of dry layer mass transfer resistance for various pharmaceutical formulations during primary drying using product temperature profiles. Int. J. Pharm. 313.
Nellis, G.F., Klein, S.A., 2009. Radiation. In: Heat transfer. Cambridge University Press, Cambridge.
Overcashier, D.E., Patapoff, T.W., Hsu, C.C., 1999. Lyophilization of protein formulations in vials: Investigation of the relationship between resistance to vapor flow during primary drying and small-scale product collapse. J. Pharm. Sci. 88.
Patel, S.M., Doen, T., Pikal, M.J., 2010. Determination of end point of primary. AAPS PharmSciTech 11.
Pikal, M.J., 2002. Freeze drying, Encyclopedia of Pharmaceutical Technology, third ed.
Pisano, R., Capozzi, L.C., 2017. Continuous freeze-drying and its relevance to the pharma/biotech industry. Integrated Biomanufacturing III.
Rey, L., May, J.C., 2010. Freeze Drying/Lyophilization of Pharmaceutical and Biological Products, vol. 206.
Searles, J.A., Carpenter, J.F., Randolph, T.W., 2001. The ice nucleation temperature determines the primary drying rate of lyophilization for samples frozen on a temperature-controlled shelf. J. Pharm. Sci. 90.
Skinsorb. 2018. Dual chamber cartridge type.http://www.skinsorb.com/biotablets/dual-chamber-syringe.
United States Food and Drug Administration, 2004. Guidance for Industry PAT: A Framework for Innovative Pharmaceutical Development, Manufacuring, and Quality Assurance.
Van Bockstal, P.J., 2016. Mechanistic modelling of infrared mediated energy transfer during the primary drying step of continuous freeze-drying process. Eur. J. Pharm. Biopharm. 114.
Van Bockstal, P.-J., De Meyer, L., Corver, J., Vervaet, C., De Beer, T., 2016. Noncontact infrared-mediated heat transfer during continuous freeze-drying of unit doses. J. Pharm. Sci.
Van Bockstal, P.-J., Corver, J., De Meyer, L., Vervaet, C., De Beer, T., 2018. Thermal imaging as a non-contact in-line process analytical tool for product temperature monitoring during continuous freeze-drying of unit doses. Anal. Chem.
Van Der Wel Peter. Active Freeze Dryer als alternatief voor tray-droger, Tech. rep.
Wang, W., 2000. Lyophilisation and development of solid pharmaceuticals. Int. J. Pharm. 203.
Werk, T., Ludwig, I.S., Luemkemann, J., Mahler, H.C., Huwyler, J., Hafner, M., 2016. Technology, applications, and process challenges of dual chamber systems. J. Pharm. Sci. 105 (1), 4–9.
Werk, T., Ludwig, I.S., Luemkemann, J., Huwyler, J., Mahler, H.-C., Haeuser, C.R., Hafner, M., 2016. New processes for freeze-drying in dual-chamber systems. PDA J. Pharm. Sci. Technol. 70 (3), 191–207.